Peer-reviewed version available at *Catalysts* **2019**, *9*, 100; doi:10.3390/catal9010100

Insights into the nature of hydroxyl groups and Zn species over defective HZSM-5 zeolite supported zinc catalysts prepared by chemical liquid deposition (CLD) with $Zn(CH_2CH_3)_2$

Long Lin[1], Xiaotong Zhang[1], Ning He[1], Jiaxu Liu[1,*], Qin Xin[2], Hongchen Guo[1]

1 State Key Laboratory of Fine Chemicals and School of Chemical Engineering, Dalian University of Technology, No. 2 Linggong Road, Dalian 116024, PR China

2 State Key Laboratory of Catalysis, Dalian Institute of Chemical Physics, Chinese Academy of Sciences, Dalian 116023, PR China

* Correspondence: liujiaxu@dlut.edu.cn; Tel.: +86--411-8498-6162; Fax: +86--411-8498-6162

Abstract: A series of defective ZSM-5 zeolites (~300 nm, SiO_2/Al_2O_3 ratio of 55, 100, 400 and 950) were intentionally prepared and systematically studied by XRD, SEM, ^{29}Si MAS NMR, argon physisorption, NH_3-TPD and FT-IR technologies. The nature, the amount and the accessibility of the acid sites of defective ZSM-5 zeolites are greatly different from reported ZSM-5 zeolites with perfect crystal structure. The co-existed strong Brønsted acid sites (Si(OH)Al) and weak Brønsted acid sites (hydroxyl nests) over defective ZSM-5 zeolites might lead to unique catalytic function. $Zn(C_2H_5)_2$ was grafted onto defective ZSM-5 zeolites through chemical liquid deposition (CLD) method. Interestingly, FT-IR spectroscopy studies find that $Zn(C_2H_5)_2$ was preferentially grafted on the hydroxyl nests with weak acidity rather than the Si(OH)Al groups with strong acidity over different defective ZSM-5 zeolites. Particularly, home-built *operando* dual beam FTIR-MS was applied to study the catalytic performance of Zn species locating at different sites of defective ZSM-5 zeolites under *n*-hexane transformation. Results show that Zn species grafted over hydroxyl nests obtain better dehydrogenation performance than Zn species over framework aluminum. This study provides guidance for the

rational design of highly efficient alkane dehydrogenative aromatization catalysts.

Keywords: defective ZSM-5; hydroxyl nests; Si(OH)Al; $Zn(C_2H_5)_2$, chemical liquid deposition; *operando* dual beam FT-IR spectroscopy

1. Introduction

The formation of a "hydroxyl-nest defect" over silica-alumina zeolites, consisting of 4 silanols, that substitute for [AlO_4] tetrahedron, was firstly proposed by Barrer and Makki [1]. After that, Zecchina performed systematically theoretical calculation and found that the hydroxyl nests can be represented as one or more missing [SiO_4] units in the zeolitic framework. In order to the preserve the stoichiometry, the obtained microcavities are saturated with neighboring OH groups which are close enough to generate hydroxyl chains interacting through hydrogen bonding [2]. Hydroxyl nests can form during the synthesis of zeolites, research has found that the amount of internal defects in zeolites depends reversely upon the concentration of Na and Al impurities [3], meanwhile it can be controlled by altering the silica source or changing fluoride as the mineralizing agent [4]. Hydroxyl nests can also form in aluminosilicate or borosilicate zeolite materials by leaching or by steaming at high temperatures [5].

Zeolite material with hydroxyl nests is less hydrophobic than the zeolite with intact structure due to the presence of high density of internal OH groups [6]. Heitmann et al [7] found these internal hydroxyl nests obtain very weak acidity which is suitable for special applications. For example, Beckman rearrangement reaction (cyclohexanone oxime to form ε-caprolactam in gas phase at 350 ^{o}C) could be catalyzed by the hydroxyl nests over silicalite-1 with high activity and selectivity [8]. Besides providing weak acidity, the hydroxyl nests could also provide active sites and space for the grafting of

heteroatoms such as Sn, Ti and B, etc [9]. As we all known, the preparation of heteroatom substituted silica-alumina zeolites by directly synthesis is at low efficiency such as the preparation of Sn-Beta and TS-1[10,11]. The preparation procedure is usually complex and needs to be controlled strictly. In comparison, grafting heteroatoms over hydroxyl nests by post-treatment could be operated at much milder conditions.

The special property of hydroxyl nests has been known for decades, however, the application of them has only been restricted in the Beckmann rearrangement. Jia et al [12] reported the hydroxyl nests are responsible for the rapid deactivation of ZSM-5 zeolite in methanol conversion. The hydroxyl nests accelerate the secondary reaction and coke formation side-reactions [13]. HZSM-5 zeolite with MFI structure (0.55*0.55 nm zigzag, 0.55*0.57 nm straight channel) [14] has been widely applied in many heterogeneous catalytic processes [15]. The well-developed porous structure with high surface area and strong acidity endows the extraordinary performance of HZSM-5 as successful solid acid catalyst. The acidity of HZSM-5 originates from the existence of framework aluminum species. Usually, the Si(OH)Al Brønsted acid sites located at the intersection of straight channel and zigzag channel of HZSM-5 zeolite obtain the strongest acidity while the Si(OH)Al Brønsted acid sites located at other sites obtain little weaker acidity. In general, the acid strength of HZSM-5 originates from the framework aluminum species (Si(OH)Al) is strong and the attenuation by post-treatment methods such as dealumination and ion-exchange by base metals is widely studied [16,17]. Considering the weak acidity of hydroxyl nests, by regulating the ratio of hydroxyl nests to Si(OH)Al groups, we could prepare HZSM-5 zeolites with tunable acidity obtaining strong and weak acid sites

simultaneously. These HZSM-5 zeolites could be named as defective zeolites and are expected to show novel catalytic properties.

In this study, a series of defective ZSM-5 zeolites with different SiO_2/Al_2O_3 ratio and hydroxyl nests content (~300 nm, SiO_2/Al_2O_3 ratio of 55, 100, 400 and 950) were intentionally prepared. Since the Zn modified HZSM-5 zeolites have been extensively studied and testified to be effective in the aromatization of short-chain hydrocarbons [18-20]. $Zn(C_2H_5)_2$ was grafted onto these defective ZSM-5 zeolites through CLD method. We find that $Zn(C_2H_5)_2$ was preferentially grafted on the hydroxyl nests with weak acidity rather than on the Si(OH)Al groups with strong acidity over different defective ZSM-5 zeolites. The Zn species grafted over hydroxyl nests obtain better dehydrogenation performance than Zn species over framework aluminum species.

2. Result and discussion

2.1. Defective HZSM-5 zeolites with different SiO_2/Al_2O_3 ratios

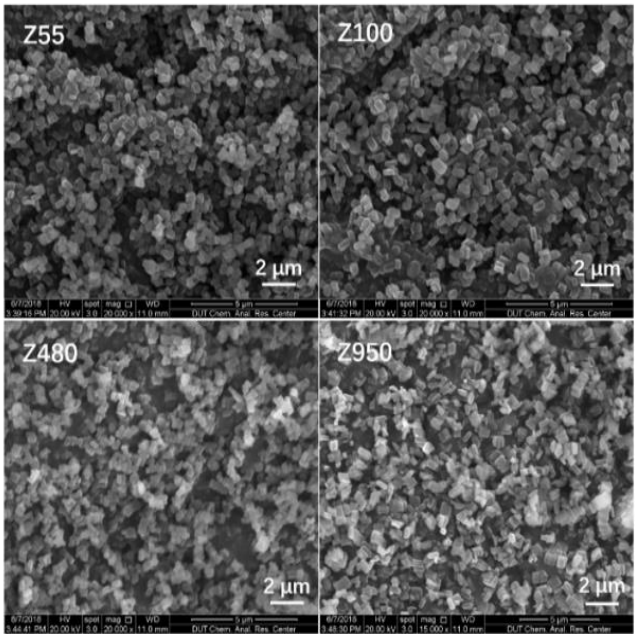

Figure 1. SEM images of defective ZSM-5 zeolites with different SiO_2/Al_2O_3 ratios.

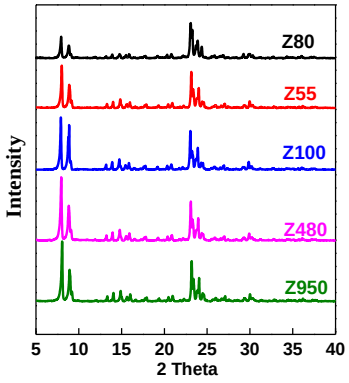

Figure 2. XRD patterns of Z80 and defective ZSM-5 zeolites with different SiO_2/Al_2O_3 ratios. Z80 was purchased from Zeolyst company (CBV8014) as reference.

Table 1. Textural properties of ZSM-5 zeolites with different SiO_2/Al_2O_3 ratios.

Samples	SiO_2/Al_2O_3	BET (m^2/g)	Smicro (m^2/g)	Vtotal (cm^3/g)	Vmicro (cm^3/g)	Crystallinity (%)
Z80	80	405	332	0.25	0.13	100
Z55	55	395	362	0.20	0.13	89.84
Z100	100	417	335	0.24	0.13	95.01
Z480	480	437	397	0.23	0.15	98.30
Z950	950	426	382	0.23	0.14	98.31

Note: S_{BET}, BET surface area was calculated by the Brunauer-Emmett-Teller (BET) method; Vmicro, micropore volume was determined by t-plot; Vmeso, mesopore volume was determined by Vtotal-Vmicro; the relative crystallinity was estimated by comparing the total XRD peak area of a zeolite sample in the range of 2 theta from 22 to 25° with that of the parent HZSM-5 having the strongest diffraction intensity.

The morphology of prepared ZSM-5 zeolites with different SiO_2/Al_2O_3 ratios was determined by SEM. As shown in Figure 1, all the crystals of these samples are in coffin shape and have a homogeneous crystal size of around 300 nm. The XRD patterns of as-prepared ZSM-5 zeolites with different SiO_2/Al_2O_3 ratios are shown in Figure 2. In order to determine the relative crystallinity of these zeolites, the commercial ZSM-5 zeolite (Z80, produced by Zeolyst) with SiO_2/Al_2O_3 ratio of 80 was applied as reference. The typical diffraction peaks of MFI type structure at 7.96, 8.83, 23.18, 23.99 and 24.45° were observed over all of these samples [21]. The Z55 sample obtained the lowest relative crystallinity of 89.84%. In comparison, other as-prepared ZSM-5 zeolites (Z100, Z450 and Z900) obtain similar crystallinity with the commercial Z80 zeolite. For the as-prepared ZSM-5 zeolites, the surface area and pore volume increased with SiO_2/Al_2O_3 ratio (Table 1). Except for Z55, the other prepared zeolites obtain similar surface area and pore volume to that of Z80 reference. These results suggest that the as-prepared ZSM-5 zeolites with high SiO_2/Al_2O_3 ratio are well-crystallized zeolites with similar porous

structure of commercial Z80 reference.

To our surprise, although the textual properties of the as-prepared ZSM-5 zeolites and Z80 reference are similar, their chemical properties are totally different. The acidity of these samples are characterized by OH-FTIR and NH_3-TPD (Figure 3 and Figure S1). Figure 3a shows the characteristic IR spectra of the as-prepared ZSM-5 zeolites in the range of 3800-3200 cm^{-1}, which corresponds to the OH-stretch vibrations in ZSM-5 zeolites. Three adsorption bands could be identified from the spectra. The band at 3720 cm^{-1} belongs to the free internal silanol (SiOH) [22]. The band at 3740 cm^{-1} can be associated with the isolated external silanol (SiOH), and the broad SiOH band centered at around 3500 cm^{-1} is generally ascribed to hydroxyl nests that consist of a number of silanol groups interacting through extended hydrogen bonding [22-24]. The intensity of hydroxyl nests over different prepared ZSM-5 zeolites is great stronger than the other peaks. One thing needs to be paid attention is that the absorbance of framework aluminum species Si(OH)Al (3610 cm^{-1}) [22,25] over these zeolites do not show up. These Si(OH)Al species might be overlapped by hydroxyl nests. Based on these OH-FTIR results, the as-prepared ZSM-5 zeolites containing substantial amount of hydroxyl nests were defined as defective ZSM-5 zeolites.

The NH_3-TPD profiles of defective ZSM-5 zeolites with different SiO_2/Al_2O_3 ratios are shown in Figure 3b. Generally, the NH_3-TPD profiles of HZSM-5 zeolites have two typical desorption peaks: one centered at about 270 ^oC (low-temperature peak) and one other at 400 ^oC (high-temperature peak). The low-temperature peak is associating with acid sites obtaining weak acidity [26-28]. The high-temperature peak is associating with acid sites obtaining strong acidity [29,30]. The total acid amount of these samples decreased gradually with the increasing of SiO_2/Al_2O_3 ratio. For Z80 reference,

the absorbance of framework aluminum species Si(OH)Al (3610 cm^{-1}) is great stronger than that of the SiOH groups (Figure S1a). The strength and total amount of acid sites over Z80 is considerably larger than that of defective ZSM-5 zeolites.

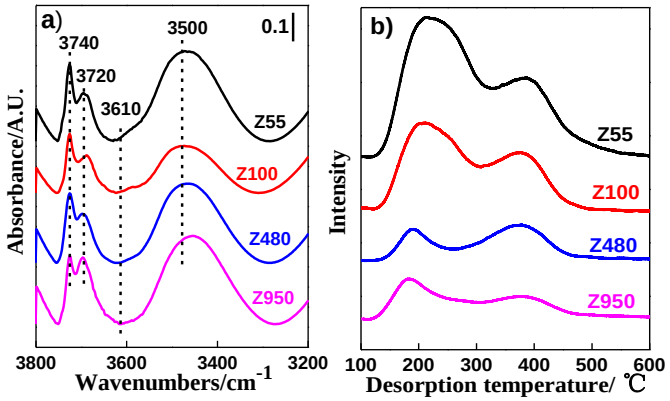

Figure 3. Acidity of defective ZSM-5 zeolites with different SiO_2/Al_2O_3 ratios. a) FT-IR spectra of hydroxyl groups, b) NH_3-TPD profiles.

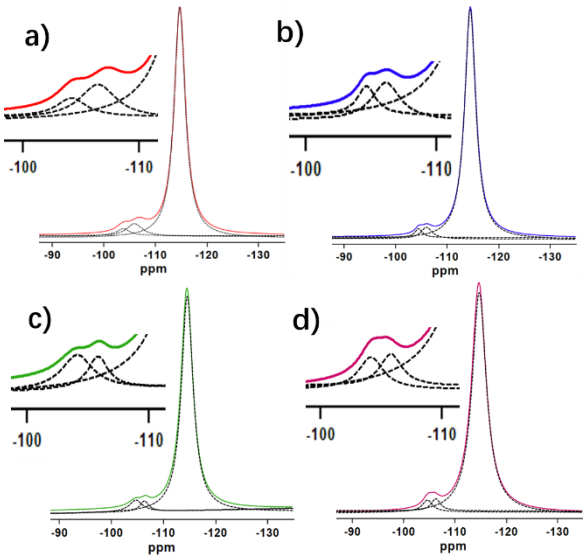

Figure 4. ^{29}Si MAS NMR spectra of defective ZSM-5 zeolites: a) Z55, b) Z100, c) Z480, d) Z950.

The ^{29}Si MAS NMR spectra of defective zeolites with different SiO_2/Al_2O_3 ratios (Figure 4) show three similar resonances. The strongest resonance at -116 ppm corresponds to $Si(OSi)_4$ species in the framework of zeolites [31].

The resonance at -106 ppm is assigned to $(AlO)_1Si(OSi)_3$ species [32] and the resonance at -102 ppm is assigned to $(OH)Si(OSi)_3$ species [33]. The relative intensity of $(AlO)_1Si(OSi)_3$ to $(OH)Si(OSi)_3$ over Z55 is great higher than the other samples which results from its high content of framework aluminum species (Si(OH)Al). For the other defective ZSM-5 zeolites with high SiO_2/Al_2O_3 ratios, although the OH-FTIR didn't find the Si(OH)Al groups, the Si(OH)Al indeed existed but greatly influenced by the hydroxyl nests.

Abovementioned results indicate that these defective ZSM-5 zeolites contain comparable amount of hydroxyl nests with weak acidity. The abundant surface OH groups and tunable acidity could endow defective ZSM-5 zeolites novel application.

2.2. Defective HZSM-5 supported Zn catalysts prepared by chemical vapor deposition (CLD) with $Zn(C_2H_5)_2$

In order to explore the potential of defective ZSM-5 zeolites as working catalyst and disclose the catalysis function of hydroxyl nests. $Zn(C_2H_5)_2$ was grafted onto these defective ZSM-5 zeolites through CLD method. The interaction between $Zn(C_2H_5)_2$ reactant and hydroxyl groups over zeolites is a stoichiometric reaction [34,35] as shown in Scheme 1. The Zn/Al ratio over Zn grafted different defective ZSM-5 zeolites was controlled at the same level. It is clear that, $(ZnOH)^+$ species could form during zeolite modified by $Zn(C_2H_5)_2$ from ^1H MAS NMR result (Fig S2). Joseph et al [36] found that $(ZnOH)^+$ species are not thermally stable and easily undergo dehydration, by coupling of $(ZnOH)^+$ species with acidic OH groups to form water and a bridging Zn^{2+} cation. Therefore, Zn^{2+} is the main type of zinc species in the samples modified by $Zn(C_2H_5)_2$.

OH-FTIR was applied to reveal the relative activity of different hydroxyl groups with $Zn(C_2H_5)_2$ over defective ZSM-5 zeolites. As the results shown

in Figure 5, for all the defective ZSM-5 zeolites, the $Zn(C_2H_5)_2$ reactant preferentially reacted with the hydroxyl nests (the broad absorbance centered at 3500 cm^{-1}). For Z55, the absorbance of hydroxyl nests of Zn/ZSM-5 gradually decreases with the increasing of Zn/Al ratio. Meanwhile, the absorbance of internal Si(OH) and external Si(OH) groups at 3720 cm^{-1} and 3740 cm^{-1}, respectively also decrease as the increasing Zn/Al ratio. Interestingly, when the absorbance of hydroxyl nests vanishes, the absorbance of the Si(OH)Al at 3610 cm^{-1} shows up. Further increasing Zn/Al ratio, these Si(OH)Al absorbance gradually decreases. These results suggest that the activity of $Zn(C_2H_5)_2$ reacts with different hydroxyl groups follows the sequence of hydroxyl nest ≧ external SiOH ≧ internal SiOH > Si(OH)Al. Similar phenomena have been found over defective ZSM-5 zeolites with high SiO_2/Al_2O_3 ratios. Abovementioned results suggest that Zn species were preferentially grafted on the hydroxyl nests with weak acidity rather than on the Si(OH)Al groups with strong acidity over defective ZSM-5 zeolites. The as-prepared Zn-defective ZSM-5 catalysts might obtain novel catalytic function.

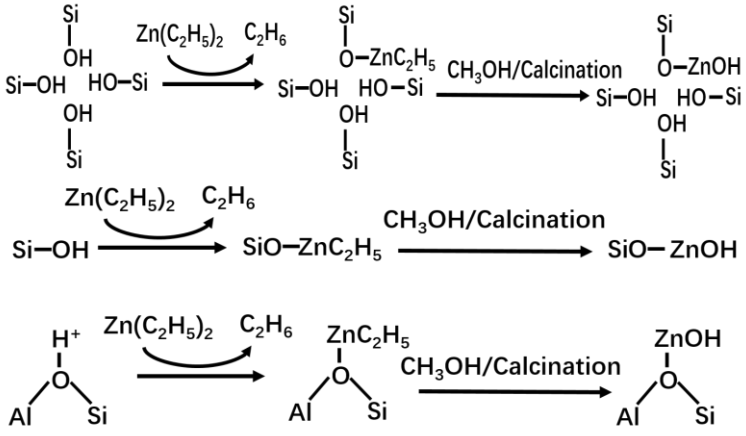

Scheme 1. The stoichiometric reaction of $Zn(C_2H_5)_2$ modifier and hydroxyl groups over zeolites.

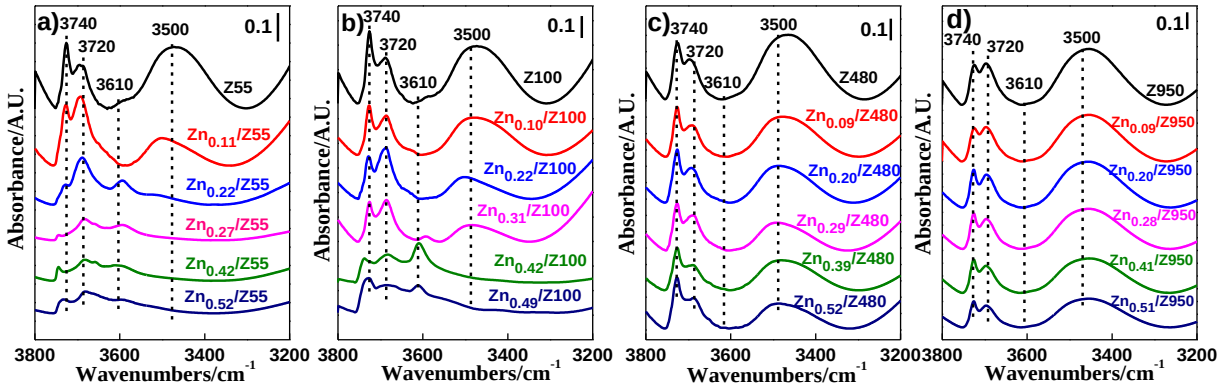

Figure 5. FT-IR spectra of hydroxyl groups on $Zn(C_2H_5)_2$ grafted defective ZSM-5 zeolites with different Zn loading: a) Zn/Z55, b) Zn/Z100, c) Zn/Z480, d) Zn/Z950.

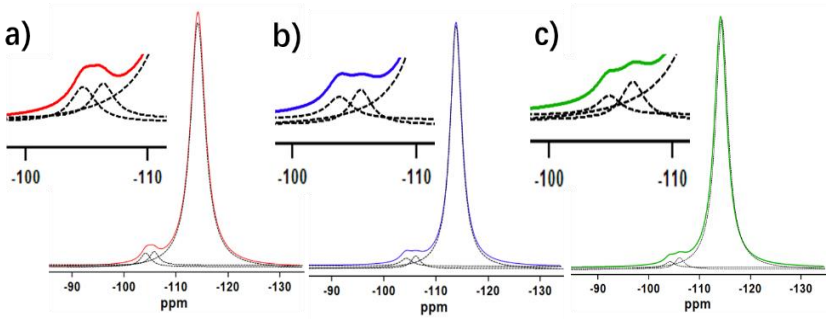

Figure 6. ^{29}Si MAS NMR spectra of Zn modified a) Z950, b) $Zn_{0.20}$/Z950, c) $Zn_{0.51}$/Z950 zeolites.

Figure 6 shows the ^{29}Si MAS NMR spectra of Zn modified Z950 zeolites. The strongest resonance at -116 ppm corresponding to $Si(OSi)_4$ species over these samples is at the same level. While, the relative intensity of $(AlO)_1Si(OSi)_3$ to $(OH)Si(OSi)_3$ over Z950 increased with the amount of grafted Zn. This suggest that Zn species was preferentially grafted on the hydroxyl nests over the defective ZSM-5 zeolite with high SiO_2/Al_2O_3 ratio.

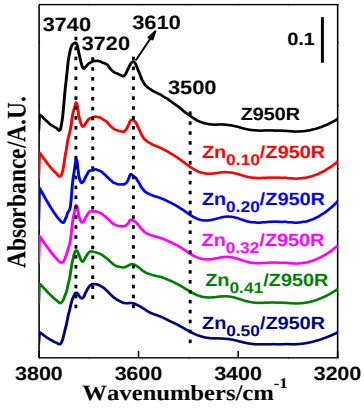

Figure 7. FT-IR spectra of hydroxyl groups on $Zn(C_2H_5)_2$ grafted Z950R zeolite with different Zn loading.

The results of FT-IR (Figure 5) and ^{29}Si MAS NMR (Figure 6) show that $Zn(C_2H_5)_2$ preferentially interact with hydroxyl nests on defective ZSM-5 zeolites. In order to selectively graft zinc species on Si(OH)Al, eliminating the hydroxyl nests over defective ZSM-5 zeolite is necessary [34]. Defective Z950 zeolite was treated by $(NH_4)_2SiF_6$ solutions to prepare defect-free ZSM-5 zeolite named as Z950R [37], then $Zn(C_2H_5)_2$ was grafted onto Z950R to obtain Zn/Z950R. As the OH-FTIR spectra shown in Figure 7, the hydroxyl nests (absorbance centered at around 3500 cm^{-1}) disappeared while the Si(OH)Al species (absorbance at 3610 cm^{-1}) shown up. These results suggest that the defects of Z950 were fully repaired after AHFS treatment and the main active sites of the as-prepared Z950R are Si(OH)Al and SiOH (internal and external). After $Zn(C_2H_5)_2$ grafting, the absorbance at 3610 cm^{-1} corresponding to Si(OH)Al gradually decreased until fully disappeared when the Zn/Al ratio increased to 0.5. While the absorbance at 3720 and 3740 cm^{-1} corresponding to SiOH didn't change. This phenomenon is completely different with that of $Zn(C_2H_5)_2$ grafting Z950. For Zn/Z950R with different Zn loadings, most of the Zn^{2+} located over framework aluminum species.

While, for Zn/Z950 with different Zn loadings, most of the Zn^{2+} located over the hydroxyl nest.

2.3. Properties of Zn species located in hydroxyl nests versus in Si(OH)Al

2.3.1 Acid properties of Zn species located in hydroxyl nests versus in Si(OH)Al

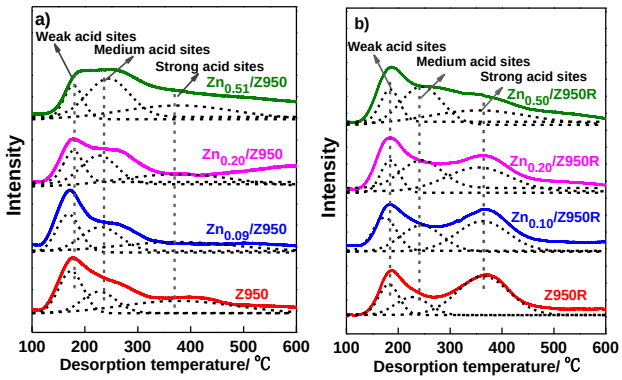

Figure 8. NH_3-TPD profiles of $Zn(C_2H_5)_2$ grafted over Z950 (a) and Z950R (b) catalysts.

The repairing of the framework of Z950 leads to the disappearance of hydroxyl nests and emergence of Si(OH)Al species (Figure 7) increasing the total amount of acid sites especially the acid sites with strong acid strength according to NH_3-TPD results (Figure 8). For Z950, after $Zn(C_2H_5)_2$ grafting, the amount of acid sites with medium strength gradually increased. For Z950R, after $Zn(C_2H_5)_2$ grafting, the amount of acid sites with strong strength gradually decreased at the increase of acid sites with medium strength. The reason might lie in the ion exchange reaction between H^+ from Si(OH)Al and Zn^{2+} which shifts the acid strength from strong to medium [38].

2.3.2 Catalytic performance of Zn species located in hydroxyl nests versus in Si(OH)Al

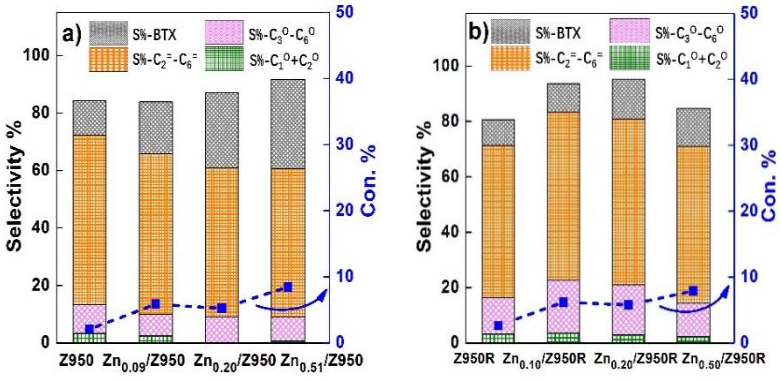

Figure 9. Products selectivity of n-hexane aromatization on (a) Zn/Z950 and (b) Zn/Z950R catalysts in pulse micro-reactor. Reaction conditions: T = 600 ℃ (Zn/Z950) & 500 ℃ (Zn/Z950R), P = 101.33 kPa.

The catalytic performance of as-prepared Zn/950 and Zn/950R sample was evaluated by n-hexane conversion as model reaction. The target is to figure out the catalytic functions of Zn^{2+} locating at ion exchange position and hydroxyl nests. The n-hexane conversion tests of Zn/Z950 and Zn/Z950R were performed in pulse micro-reactor under atmospheric pressure. The product distributions of Zn/Z950 and Zn/Z950R were shown in Table S1. For Zn/Z950 (Figure 9), the selectivity of BTX apparently increased at the expense of the selectivity of C2-C6 olefin with Zn/Al ratio. While the selectivity of methane and ethane exhibited adverse trend. These results suggest that Zn^{2+} located at hydroxyl nest could catalyze the dehydrogenative aromatization of n-hexane significantly. However, for Zn/Z950R, the selectivity of BTX slightly increased with Zn/Al ratio. These results show that Zn species located in hydroxyl nests obtain better dehydrogenation performance than Zn species over framework aluminum species.

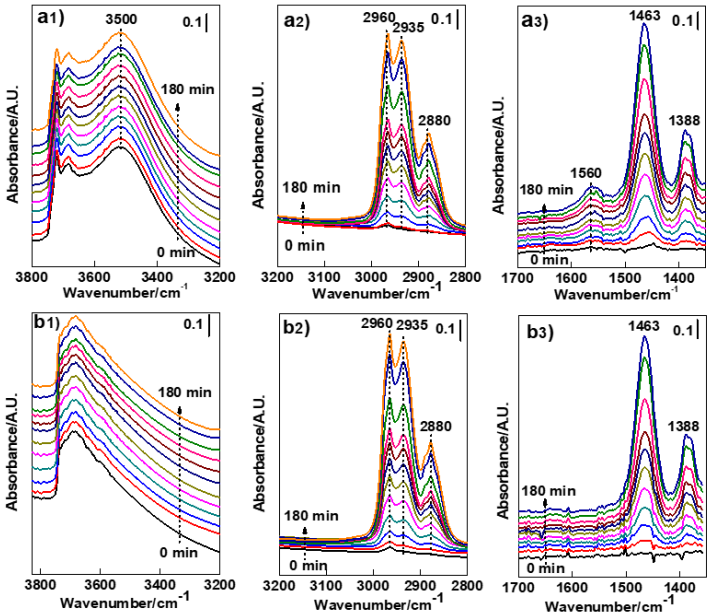

Figure 10. Selected FT-IR profiles of n-hexane aromatization over $Zn_{0.51}$/Z950 (a) and $Zn_{0.50}$/Z950R (b) catalysts obtained over DB-FTIR spectrometer. Reaction conditions: T = 300 ℃, P = 101.33 kPa, n-hexane was carried into IR-cell reactor by N_2 (10ml/min), GHSV = 220 h^{-1}.

Operando DB-FTIR spectroscopy study was employed to know more about the catalytic functions of Zn^{2+} locating at ion exchange position and hydroxyl nests in *n*-hexane transformation. To do this study, an *operando* spectroscopy system was built according to described method [39]. The overall three-dimensional FTIR profiles of $Zn_{0.51}$/Z950 (a) and $Zn_{0.50}$/Z950R (b) in 180 min are completely recorded by dual beam FT-IR spectrometer and shown in Fig S3. In order to get more detailed information, the selected FT-IR profiles (1300-1700, 2800-3200 and 3200-3800 cm^{-1}) are displayed in Fig 10. Noticeably, the sample of $Zn_{0.51}$/Z950 (a) has a significant absorption peak at 1560 cm^{-1}, according to the literature data, this peak most likely due to olefins with internal double bond, polyenic species or precursors of aromatic compounds [40,41]. These results suggest that Zn^{2+} located at hydroxyl nest could catalyze the dehydrogenative aromatization of n-hexane significantly.

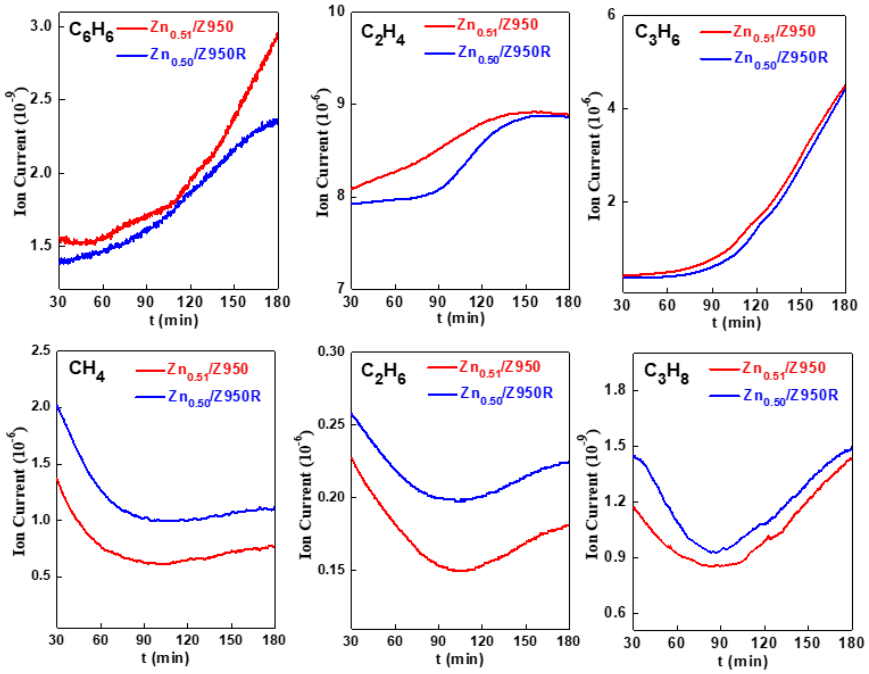

Figure 11. Mass spectra of n-hexane aromatization on $Zn_{0.51}$/Z950 and $Zn_{0.50}$/Z950R catalysts. Reaction conditions: T = 300 ℃, P = 101.33 kPa, n-hexane was carried into IR-cell reactor by N_2 (10ml/min), GHSV = 220 h^{-1}.

During the above FT-IR experiment, the products were monitored by mass spectrometer, as shown in Fig 11, $Zn_{0.51}$/Z950 exhibits higher olefins and aromatics composition than $Zn_{0.50}$/Z950R, which indicates that Zn species located in hydroxyl nests obtained better dehydrogenation and aromatization properties than Zn species located in framework aluminum species. These results coincide quite well with the catalytic tests of pulse micro-reactor and *operando* dual beam FT-IR.

3. Materials and Methods

3.1. Materials

Nano-sized defective NaZSM-5 zeolite with SiO_2/Al_2O_3 molar ratio of 55, 100, 480 and 950 were manufactured by Dalian Ligong Qiwangda Chemical Technology (Dalian, China). The HZSM-5 was obtained by exchanging the NaZSM-5 twice at 80 ºC with 1 M solution of NH_4NO_3 with a liquid-to-solid weight ratio of 5 for 1 h. The sample was filtered and washed with deionized water each time after exchange, and finally dried at 110 ºC for 12 h and then calcined at 540 ºC in flowing dry air for 6 h. The prepared samples were named as Z55, Z100, Z480 and Z950.

Commercial NH_4ZSM-5 zeolite with SiO_2/Al_2O_3 molar ratio of 80 (CBV8014) was purchased from Zeolyst International to compare with the defective ZSM-5 zeolites. The ZSM-5 in hydrogen form was obtained by calcined at 540 ºC in flowing dry air for 6 h, named as Z80.

In order to illustrate the role of defective sites over HZSM-5 in catalysis, the defective sites of ZSM-5 zeolite with SiO_2/Al_2O_3 ratio of 950 was repaired by $(NH_4)_2SiF_6$ post treatment according to the publication [37].

3.2. Zn/ZSM-5 prepared by chemical liquid deposition (CLD) with $Zn(C_2H_5)_2$

Zn was introduced into HZSM-5 by CLD with $Zn(C_2H_5)_2$. All the preparations were performed in a nitrogen-flushed glovebox. An amount of 1 g of dehydrated zeolite (calcination in muffle at 540 ºC for 3 hours) was suspended in 50 mL of anhydrous n-hexane in a 100-mL conical flask with stopper. $Zn(C_2H_5)_2$ (1.0 M solution in n-hexane) was slowly added to the mixture via stirring. The mixture was stirred at room temperature for 20 h and centrifuged. The isolated solid was then stirred in 50 mL of anhydrous methanol for 4 h at room temperature, centrifuged; separated solid was dried at 110 ºC for 12 h, and then calcined at 540 ºC for 3 h. The resulting zeolite catalysts are designated in the following manner: Zn_X/Y, where X is the practical molar ratio of Zn and Al, Y is the practical SiO_2/Al_2O_3 molar ratios in the catalyst.

3.3. Characterization

The materials were characterized by scanning electron microscopy (SEM); X-ray fluorescence (XRF); inductively coupled plasma optical emission spectrometry (ICP-OES); Argon physisorption; X-ray diffraction (XRD); temperature programmed desorption of NH_3 (NH_3-TPD); fourier transform infrared spectroscopy (FT-IR) and high resolution ^{29}Si magic angle spinning nuclear magnetic resonance (MAS-NMR).

The scanning electron microscopy (SEM) image to characterize the surface morphology of the as-prepared zeolite sample was taken on a Quanta 450 scanning electron microscope.

X-ray fluorescence (XRF) measurements were performed with a Bruker S8 TIGER spectrometer to determine the bulk silicon-to-aluminum ratio.

The molar ratio of Zn and Al was analyzed by inductively coupled plasma optical emission spectrometry (ICP-OES) using an optima 2000DV

instrument.

Argon physisorption was conducted on a Micromeritics ASAP 2020 instrument at -196 ℃ to obtain textural information. Prior to the measurement, the samples (380-830 μm sieve fraction) were degassed at 350 ℃ for 6 h. The surface area was calculated by the Brunauer-Emmett-Teller (BET) method using the adsorption branch in the p/p_o range from 0.10 to 0.15, and the pore volumes were estimated at p/p_o of 0.99, while the micro-and mesoporosity was discriminated by the *t*-plot method.

X-ray diffraction (XRD) patterns were obtained by a Rigaku D/max-2004 diffractometer with Cu Kα radiation (40 kV, 100 mA) at a 0.02 °min^{-1} (2θ) scanning speed. By assuming that the zeolite sample having the largest peak area in the range of 2 theta from 22 ° to 25 ° as a reference had a crystallinity of 100% (here it was Z80), the relative crystallinity of each zeolite sample was then estimated by comparing its total peak area in this 2 theta range with that of the reference sample.

NH_3-TPD measurements were carried out in a self-designed flow apparatus using TCD detector. Approximately 150 mg of the zeolite sample was used in each measurement, which was first pretreated at 600 ºC for 1 h in a helium stream (30 ml/min) and then cooled down to 100 ºC. Saturated adsorption of NH_3 on the zeolite sample was then achieved by pulse gaseous NH_3 into the sample tube. After that, the physically adsorbed NH_3 was removed by flushing the sample tube with a helium flow (30 ml/min) at 100 ºC for 2 h. To get the NH_3-TPD profile, the zeolite sample was then heated up from 100 to 600 ºC at a ramp of 17 ºC/min; the amount of NH_3 released during the heating for desorption was measured by a thermal conductivity detector (TCD).

The spectra of the surface hydroxyl (-OH) vibration were obtained with a

Nicolet is10 FT-IR spectrometer. The zeolitic samples were pressed into a self-supporting thin wafer (approximately 15 mg) and decontaminated at 400 ℃ under vacuum (10^{-3} Pa) for 4 h in a quartz IR cell equipped with CaF_2 windows. After the pretreatment, the cell was cooled down to room temperature for the sample measurements. The spectrum was recorded from 4000 to 400 cm^{-1} with an optical resolution of 4 cm^{-1}. The hydroxyl vibration spectra were obtained by subtracting the background spectrum (recorded with an empty IR cell in the absence of sample) from the measured sample spectra.

High resolution ^{29}Si magicangle spinning nuclear magnetic resonance (MAS-NMR) spectra were recorded using an Agilent DD2 500 spectrometer.

3.4. Catalytic tests

3.4.1. Pulse micro-reactor

N-hexane conversion tests were performed in a pulse micro-reactor under atmospheric pressure. The catalytic measurements were carried out at 500 and 600 °C respectively, the catalyst sample was pressurized to wafers and then crushed and sieved to 20-40 mesh before use. In a typical run, 200 mg of the zeolite catalyst was loaded, then 1 uL n-hexane was injected into the reactor with the contact reaction time about 0.15 s. The product composition was analyzed by an online gas chromatograph (TECHCOMP GC7900) equipped with a PLOT-Q column (30 m×4 mm) with a flame ionization detector.

The *n*-hexane conversion ($C_{n\text{-hexane}}$) and product selectivity (S_i) were calculated using the following equations:

$$C_{n\text{-hexane}} = (\sum A_i - A_{n\text{-hexane}})/\sum A_i \times 100\% \quad (1)$$

$$S_i = A_i/(\sum A_i - A_{n\text{-hexane}}) \times 100\% \quad (2)$$

where A_i and $A_{n\text{-hexane}}$ are the corrected chromatographic areas of a specific

compound and residual *n*-hexane, respectively.

3.4.2. Home-built *operando* dual beam FTIR-MS

In this case, a self-developed dual beam FT-IR spectrometer, a dual beam IR-cell reactor and an on-line mass spectrometer were used to construct the *operando* spectroscopy system. Catalyst samples were pressed into self-supporting thin wafers (1 cm^2) and placed in the sample beam of the dual beam IR cell, and the reference beam was left vacant. The experiment procedures and the method to do spectrum subtraction were described elsewhere [22,39,42]. In this study, samples were pretreated in the IR-cell reactor at 400 °C for 4 h under vacuum (10^{-3} Pa). The temperature of n-hexane aromatization was carried out at 300 °C. N-hexane was carried into IR-cell reactor by nitrogen (10ml/min), GHSV = 220 h^{-1}. The spectra were recorded at a resolution of 4 cm^{-1} with 64 scans in the region of $\tilde{\nu}$ = 4000-400 cm^{-1}.

During the above FT-IR experiments the changes of the product composition have been monitored by a QMS 200 (Balzers) quadrupole mass-spectrometer. The changes in the signal intensity of the main fragments of benzene, ethylene, propene, methane, ethane, propane and those of the possible products were simultaneously followed.

4. Conclusions

A series of defective ZSM-5 with different SiO_2/Al_2O_3 ratio were intentionally prepared and systematically titrated by $Zn(C_2H_5)_2$ to study the difference between Zn species interacting with hydroxyl nests and Si(OH)Al by FT-IR and other technologies. Results show that $Zn(C_2H_5)_2$ was preferentially grafted on the hydroxyl nests with weak acidity rather than Si(OH)Al groups with strong acidity over different defective ZSM-5 zeolites. Particularly, according to the *operando* dual beam FT-IR result, Zn species grafted on hydroxyl nests obtain better dehydrogenation performance than Zn

species grafted over framework aluminum species. This study provides guidance for the rational design of highly efficient alkane dehydrogenative aromatization catalysts.

Acknowledgments

This work was financially supported by the National Natural Science Foundation of China (21603023) and the Joint Fund Project of NSFC-Liaoning Province (U1508205).

Supplementary Materials:

Figure S1: Acidity of Z80 zeolite. a) FT-IR spectra of hydroxyl groups, b) NH_3-TPD profiles; Fig S2. ^1H MAS NMR spectrum on $Zn(C_2H_5)_2$ grafted Z950R zeolite with different Zn loading; Figure S3: The overall three-dimensional FTIR profiles of n-hexane aromatization on Zn/Z950 (a) and Zn/Z950R (b) catalysts in180 min. Reaction conditions: T = 300 ℃, P = 101.33 kPa, n-hexane was carried into IR-cell reactor by N_2 (10ml/min), GHSV = 220 h^{-1}; Table S1: Products distribution of n-hexane aromatization on Zn/Z950 and Zn/Z950R catalysts in a pulse micro-reactor. Reaction conditions: T = 500 & 600 ℃, P =101.33 kPa; Scheme S1. Schematic diagram for repairing lattice defects of ZSM-5 zeolite by $(NH_4)_2SiF_6$.

References

1. Barrer, R.M.; Makki, M.B. Molecular sieve sorbents from clinoptilolite. *Can. J. Chem.* **1964**, *42*, 1481-1487.

2. Zecchina, A.; Bordiga, S.; Spoto, G.; Marchese, L.; Petrini, G.; Leofanti, G.; Padovan, M. Silicalite characterization. Structure, adsorptive capacity, and IR spectroscopy of the framework and hydroxyl modes. *J. Phys. Chem.* **1992**, *96*, 4985-4990.

3. Bordiga, S.; Ugliengo, P.; Damina, A.; Lamberti, C.; Spoto, G.; Zecchin, A.; Spano, G.; Buzzoni, R.; Dalloro, L.; Rivetti, F. Hydroxyls nests in defective silicalites and strained structures derived upon dehydroxylation: vibrational properties and theoretical modelling. *Top. Catal.* **2001**, *15*, 43-52.

4. Trzpit, M.; Soulard, M.; Patarin, J.; Desbiens, N.; Cailliez, F.; Boutin, A.; Demachy, I.; Fuchs, A.H. The Effect of Local Defects on Water Adsorption in Silicalite-1 Zeolite: A Joint Experimental and Molecular Simulation Study. *Langmuir.* **2007**, *23*, 10131-10139.

5. Deruiter, R.; Kentgens, A.P.M.; Grootendorst, J.; Jansen, J.C.; Vanbekkum, H. Calciantion and deboronation of B-MFI single-crystals. *Zeolites*. **1993**, *13*, 128-138.

6. Heitmann, G.P.; Dahlhoff, G.; Niederer, J.P.M.; Holderich, W.F. Active Sites of a [B]-ZSM-5 Zeolite Catalyst for the Beckmann Rearrangement of Cyclohexanone Oxime to Caprolactam. *J. Catal*. **2000**, *194*, 122-129.

7. Heitmann, G.P.; Dahlhoff , G. Holderich, W.F. Catalytically Active Sites for the Beckmann Rearrangement of Cyclohexanone Oxime to ε-Caprolactam. *J. Catal*. **1999**, *186*, 12-19.

8. Forni, L.; Fornasari, G.; Giordano, G.; Lucarelli, C.; Katovic, A.; Trifiro, E.; Perri, C.; Nagy, J.B. Vapor phase Beckmann rearrangement using high silica zeolite catalyst. *PCCP.* **2004**, *6*, 1842-1847.

9. Graaff, W. N. P.; Li, G.; Mezari, B.; Pidko, E.A.; Hensen, E.J.M. Synthesis of Sn-Beta with Exclusive and High Framework Sn Content. *Chem. Cat. Chem.* **2015**, *7*, 1152-1160.

10. Corma, A.; Nemeth, L.T.; Renz, M.; valencia, S. Sn-zeolite beta as a heterogeneous chemoselective catalyst for Baeyer-Villiger oxidations. *Nature*. **2001**, *412*, 423-425.

11. Corma, A.; Domine, M.E.; valencia, S. Water-resistant solid Lewis acid catalysts: Meerwein-Ponndorf-Verley and Oppenauer reactions catalyzed by tin-beta zeolite. *J. Catal*. **2003**, *215*, 294-304.

12. Jia,Y.M.; Wang, J.W.; Zhang, K.; Liu, S.B.; Chen, G.L.; Yang, Y.F.; Ding C.M.; Liu, P. Catalytic Conversion of Methanol to Aromatics over Nanosized HZSM-5 Zeolite Modified by $ZnSiF_6$ $6H_2O$. *Catal. Sci. Technol*. **2012**, *00*, 1-3.

13. Bleken, F.L.; Barbera, K.; Bonino, F.; Olsbye, U.; Lillerud, K.P.; Bordiga, S.; Beato, P.; Janssens, T.V.W.; Svelle, S. Catalyst deactivation by coke formation in microporous and desilicated zeolite H-ZSM-5 during the conversion of methanol to hydrocarbons. *J. Catal.* **2013**, *307*, 62-73.

14. Kokotailo, G.T; Lawton, S.L; Olson, D.H. Structure of synthetic zeolite ZSM-5. *Nature.* **1978**, *272*, 437-438.

15. Venuto, P.B. Organic Catalysis Over Zeolites: A Perspective on Reaction Paths within Micropores. *Microporous. Mater.* **1994**, *2*, 297-411.

16. Jin, F.; Cui, Y.G.; Rui, Z.B. Effect of sequential desilication and dealumination on catalytic performance of ZSM-5 catalyst for pyridine and 3-picoline synthesis. *J. Mater. Res.* **2010**, *25*, 272-282.

17. Dyballa, M.; Obenaus, U.; Blum, M. Alkali metal ion exchanged ZSM-5 catalysts: on acidity and methanol-to-olefin performance. *Catal. Sci. Technol*. **2018**, *8*, 4440-4449.

18. Kazansky, V.B.; Shubbotina, I.R.; Rane, N.; van Santen, R.A.; Hensen, E.J.M. On two alternative mechanisms of ethane activation over ZSM-5 zeolite modified by Zn^{2+} and Ga^{1+} cations. *PCCP*. **2005**, *7*, 3088-3092.

19. Biscardi, J.A.; Iglesia, E. Non-oxidative reactions of propane on Zn/Na-ZSM5. *PCCP*. **1999**, *1*, 5753-5759.

20. Penzien, J.; Abraham, A.; van Bokhoven, J.A.; Jentiys, A.; Muller, T.E.; Sievers, C.; Lercher, J.A. Generation and Characterization of Well-Defined Zn^{2+} Lewis Acid Sites in Ion Exchanged Zeolite BEA. *J. Phys. Chem. B*. **2004**, *108*, 4116-4126.

21. Zecchina, A.; Bordiga, S.; Spoto, G.; Marchese, L.; Petrini, G.; Leofanti, G.; Radovan, M. Silicalite Characterization. 2. IR Spectroscopy of the Interaction of CO with Internal and External Hydroxyl Groups. *J. Phys. Chem.* **1992**, *96*, 4991-4997.

22. Liu, J.X.; He, N.; Zhou, W.; Lin, L.; Liu, G.D.; Liu, C.Y.; Wang, J.L.; Xin, Q.; Xiong, G.; Guo, H.C. Isobutane aromatization over a complete Lewis acid Zn/HZSM-5 zeolite catalyst: performance and mechanism. *Catal. Sci. Technol.* **2018**, *8*, 4018-4029.

23. Bordiga, S.; Roggero, I.; Ugliengo, P.; Zecchina, A.; Bolis, V.; Artioli, G.; Buzzoni, R.; Marra, G.; Rivetti, F.; Spano, G.; Lamberti, C. Characterisation of defective silicalites. *J. Chem. Soc. Dalton Trans.* **2000**, 3921-3929.

24. Bordiga, S.; Ugliengo ,P.; Damin, A.; Lamberti, C.; Spoto, G.; Zecchina, A.; Spano, G.; Buzzoni, R.; Dalloro, L; Rivetti, F. Hydroxyls nests in defective silicalites and strained structures derived upon dehydroxylation: vibrational properties and theoretical modelling. *Top. Catal.* **2001**, *15*, 43-52.

25. Zecchina, A.; Bordiga, S.; Spoto, G.; Scarano, D.; Petrini, G.; Leofanti, G.; Padovan, M. Low-temperature Fourier-transform infrared investigation of

the interaction of CO with nanosized ZSM5 and silicalite. *J. Chem. Soc. Faraday Trans.* **1992**, *88*, 2959-2969.

26. Bolis, V.; Busco, C.; Bordiga, S.; Ugliengo, P.; Lamberti, C.; Zecchina, A. Calorimetric and IR spectroscopic study of the interaction of NH_3 with variously prepared defective silicalites: Comparison with ab initio computational data. *Appl. Surf. Sci.* **2002**, *196*, 56-70.

27. Li, Y.N.; Liu, S.L.; Xie, S.J.; Xu, L.Y. Promoted metal utilization capacity of alkali-treated zeolite: Preparation of Zn/ZSM-5 and its application in 1-hexene aromatization. *Appl. Catal. A: Gen*. **2009**, *360*, 8-16.

28. Nishi, K.; Komai, S.; Inagaki, K.; Satsuma, A.; Hattori, T. Structure and catalytic properties of Ga-MFI in propane aromatization. *Appl. Catal. A: Gen*. **2002**, *223*, 187-193.

29. Choi, S.W.; Kim, W.G.; So, J.S.; Moore, J.S.; Liu, Y.J.; Dixit, R.S.; Pendergast, J.G.; Sievers, C.; Sholl, D.S.; Nair, S.; Jones, C.W. Propane dehydrogenation catalyzed by gallosilicate MFI zeolites with perturbed acidity. *J. Catal.* **2017**, *345*, 113-123.

30. Rodríguez-González, L.; Hermes, F.; Bertmer, M.; Rodríguez-Castellón, E.; Jiménez-López, A. The acid properties of H-ZSM-5 as studied by NH_3-TPD and 27Al-MAS-NMR spectroscopy. *Appl. Catal. A: Gen*. **2007**, *328*, 174-182.

31. Zhang, J.G.; Qian, W.Z.; Kong, C.Y.; Wei, F. Increasing para-Xylene Selectivity in Making Aromatics from Methanol with a Surface-Modified Zn/P/ZSM-5 Catalyst. *ACS Catal.* **2015**, *5*, 2982-2988.

32. Zhao, J.J.; Zhou, J.; Chen, Y.; He, Q.J.; Ruan, M.L.; Guo, L.M.; Shi, J.L.; Chen, H.R. Fabrication of mesoporous zeolite microspheres by a one-pot dual-functional templating approach. *J. Mater. Chem.* **2009**, *19*, 7614-7616.

33. Zhang, W.P.; Bao, X.H.; Guo, X.W.; Wang, X.S. A high-resolution solid-

state NMR study on nano-structured HZSM-5 zeolite, *Catal. Lett*. **1999**, *60*, 89-94.

34. Almutairi, S.M.T.; Mezari, B.; Magusin, P.C.M.M.; Pidko, E.A. Hensen, E.J.M. Structure and Reactivity of Zn-Modified ZSM-5 Zeolites: The Importance of Clustered Cationic Zn Complexes. *ACS Catal*. **2012**, *2*, 71-83.

35. Wang, K.; Cao, G.; Kennedy, G.J.; Afeworki, M.; Bare, R.E.; Hall, R.B. Pore Modification of H-SAPO-34 Using Dialkyl Zinc: Structural Characterization and Reaction Pathway. *J. Phys. Chem. C.* **2011**, *115*, 18611-18617.

36. Biscardi, J.A.; Meitzner, G.D.; Iglesia, E. Structure and Density of Active Zn Species in Zn/H-ZSM5 Propane Aromatization Catalysts. *J. Catal.* **1998**, *179*, 192-202.

37. Sohn, J.R.; Decanio, S.J.; Fritz, P.O.; Lunsford, J.H. Acid catalysis by dealuminated zeolite Y. 2. The roles of aluminum, *J. Phys. Chem.* **1986**, *90*, 4847-4851.

38. Chen, X.H.; Dong, M. Niu, X.J.; Wang, K.; Chen, G.; Fan, W.B.; Wang, J.G.; Qin, Z.F. Influence of Zn species in HZSM-5 on ethylene aromatization. *Chinese. J. Catal.* **2015,** *36*, 880-888.

39. Liu, J.X.; Wang, J.L.; Zhou, W.; Miao, C.L. Xiong, G. Xin, Q.; Guo, H.C. Construction of an operando dual-beam fourier transform infrared spectrometer and its application in the observation of isobutene reactions over nano-sized HZSM-5 zeolite. *Chinese. J. Catal*. **2017**, *38*, 13-19.

40. Ivanovaa, I.I.; Kolyagina, Y.G.; Ordomskya,V.V.; Asachenkoa, E.V.; Pasynkovab, E.M. Surface species formed during propane aromatization over Zn/MFI catalyst as determined by in situ spectroscopic techniques. *J. Mol. Catal. A: Chem.* **2009**, *305*, 47-53.

41. Flego, C.; Peratello, S.; Perego, C.; Sabatino, L.M.F.; Bellussi, G. Romano, U. Reaction and deactivation study of mesoporous silica-alumina (MSA) in propene oligomerisation. *J. Mol. Catal. A: Chem.* **2003**, *581*, 204-205.

42. Zhou, W.; Liu, J.X.; Lin, L.; Zhang, X.T.; He, N.; Liu, C.Y.; and Guo, H.C. Enhanced dehydrogenative aromatization of propane by incorporating Fe and Pt into Zn/HZSM-5 catalyst. *Ind. Eng. Chem. Res.* Just Accepted Manuscript. DOI: 10.1021/acs.iecr.8b03865.

Supplementary Materials

Insights into the nature of hydroxyl groups and Zn species over defective HZSM-5 zeolite supported zinc catalysts prepared by chemical liquid deposition (CLD) with $Zn(CH_2CH_3)_2$

Long Lin[1], Xiaotong Zhang[1], Ning He[1], Jiaxu Liu[1,*], Qin Xin[2], Hongchen Guo[1]

1 State Key Laboratory of Fine Chemicals and School of Chemical Engineering, Dalian University of Technology, No. 2 Linggong Road, Dalian 116024, PR China

2 *State Key Laboratory of Catalysis, Dalian Institute of Chemical Physics, Chinese Academy of Sciences, Dalian 116023, PR China*

** Correspondence: liujiaxu@dlut.edu.cn;* Tel.: +86-411-8498-6162; Fax: +86-411-8498-6162

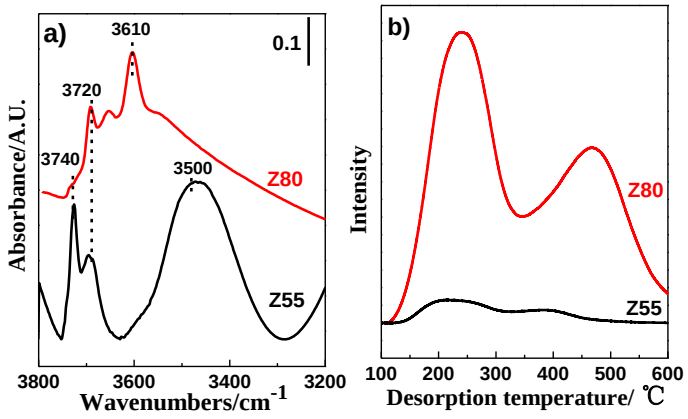

Figure S1. Acidity of Z80 zeolite. a) FT-IR spectra of hydroxyl groups, b) NH_3-TPD profile.

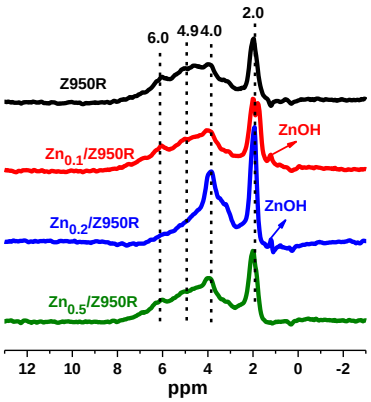

Fig S2. ^1H MAS NMR spectrum on $Zn(C_2H_5)_2$ grafted Z950R zeolite with different Zn loading.

Preprints (www.preprints.org) | NOT PEER-REVIEWED | Posted: 3 December 2018 doi:10.20944/preprints201812.0019.v1

Peer-reviewed version available at Catalysts 2019, 9, 100; doi:10.3390/catal9010100

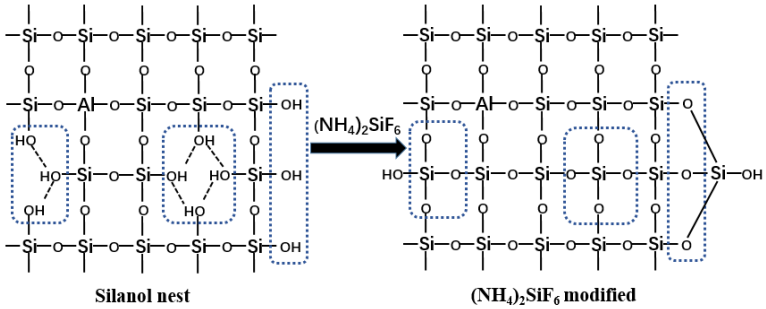

Scheme S1. Schematic diagram for repairing lattice defects of ZSM-5 zeolite by $(NH_4)_2SiF_6$.

Table S1. Products distribution of n-hexane aromatization on Zn/Z950 and Zn/Z950R catalysts in pulse micro-reactor. Reaction conditions: T = 600 ℃ (Zn/Z950) & 500 ℃ (Zn/Z950R), P = 101.33 kPa.

Cat	Con.%	S%-BTX	S%-$C_2^=$-$C_6^=$	S%-C_3^O-C_6^O	S%-C_1^O+C_2^O
Z950	2.09	11.96	58.85	10.05	3.35
$Zn_{0.09}$/Z950	5.85	17.89	56.14	7.37	2.46
$Zn_{0.20}$/Z950	5.23	26.01	52.02	8.97	0
$Zn_{0.51}$/Z950	8.48	31.13	51.65	8.25	0.71
Z950R	2.64	9.47	54.92	12.88	3.41
$Zn_{0.10}$/Z950	6.19	10.18	60.74	19.06	3.72
$Zn_{0.20}$/Z950R	5.78	14.36	59.86	17.99	2.94
$Zn_{0.50}$/Z950R	7.89	13.69	56.53	12.17	2.41

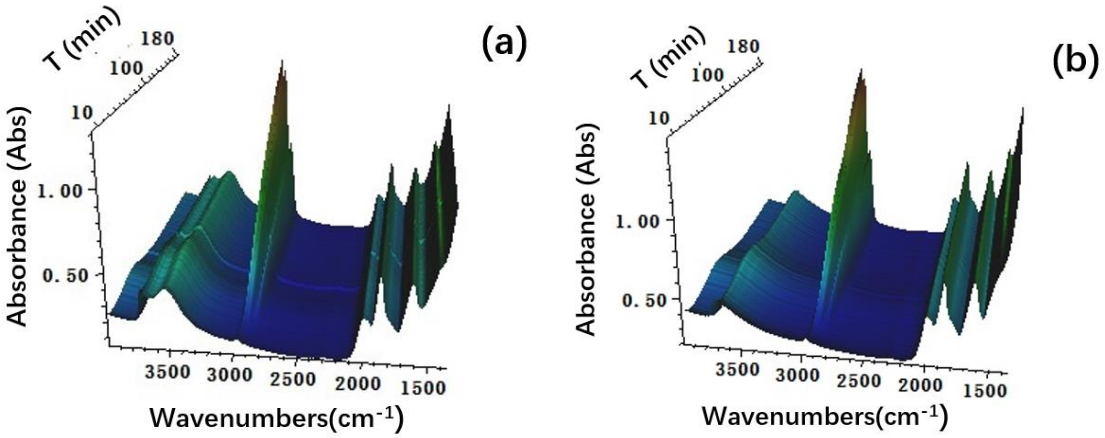

Figure S3. The overall three-dimensional FTIR profiles of n-hexane

aromatization on Zn/Z950 (a) and Zn/Z950R (b) catalysts in 180 min. Reaction conditions: T = 300 ℃, P = 101.33 kPa, n-hexane was carried into IR-cell reactor by N_2 (10ml/min), GHSV = 220 h^{-1}.